Werk

Jahr: 1979
Kollektion: fid.geo
Signatur: 8 Z NAT 2148:46
Digitalisiert: Niedersächsische Staats- und Universitätsbibliothek Göttingen
Werk Id: PPN1015067948_0046
PURL: http://resolver.sub.uni-goettingen.de/purl?PPN1015067948_0046

LOG Id: LOG_0017
LOG Titel: Finite element convection models : comparison of shallow and deep mantle convection, and temperatures in the mantle
LOG Typ: article

Übergeordnetes Werk

Werk Id: PPN1015067948
PURL: http://resolver.sub.uni-goettingen.de/purl?PPN1015067948
OPAC: http://opac.sub.uni-goettingen.de/DB=1/PPN?PPN=1015067948

Contact

Niedersächsische Staats- und Universitätsbibliothek Göttingen
Georg-August-Universität Göttingen
Platz der Göttinger Sieben 1
37073 Göttingen
Germany
Email: gdz@sub.uni-goettingen.de

J. Geophys. 46, 97–121, 1979

Journal of Geophysics

Finite Element Convection Models: Comparison of Shallow and Deep Mantle Convection, and Temperatures in the Mantle

U. Kopitzke

Institut für Geophysik und Meteorologie der Technischen Universität Braunschweig, Mendelssohnstrasse 1A, D-3300 Braunschweig, Federal Republic of Germany

Abstract. A Finite Element Method for solving the convection problem in a fluid with position-dependent Newtonian viscosity is developed, using bicubic and biquadratic spline functions on a rectangular grid. Introducing weak (less viscous) zones at the active margins of the lithosphere, dynamical mantle convection models are established which have a nearly uniform surface (plate) velocity and a satisfactory heat flux profile. A comparison of upper and deep mantle convection shows:
– a moderate increase of viscosity with depth cannot confine the flow to the upper mantle;
– in shallow depth convection models the temperature is too low inside the cell, but deep mantle convection models yield satisfactory temperatures for the upper mantle.
For that reason deep (or whole) mantle convection should be the favored hypothesis.

Key words: Mantle convection – Finite element method – Mantle geotherm.

1. Introduction

There exist two major kinds of models which describe mantle convection or basic plate tectonic processes. One kind are simple kinematic models (for example: Schubert et al., 1976; Richter and McKenzie, 1978), making assumptions on a prescribed plate velocity (and a prescribed temperature at a reference depth). These models are easy to handle – they can often be performed by analytical methods. But they do not involve the driving mechanism –, i.e., thermally caused differences of density – and so it remains unclear whether the assumptions about plate velocity and temperature are justified and consistent with the chosen rheology.

The dynamical or intrinsic convection models on the other hand need only assumptions on the distribution of heat sources and the rheological behavior of

0340-062X/79/0046/0097/$05.00

the material. They yield informations about both the velocity and the temperature field. Such models were investigated, for example, by Torrance et al. (1973), McKenzie and Roberts (1974), Houston and DeBremaecker (1975) and DeBremaecker (1977a). These models were successful in showing that mantle convection is able to drive the plates, and that cells with a large aspect ratio (the ratio between length and depth of the cell) are possible under mantle conditions.

But so far the dynamical convection models failed to incorporate the lithosphere (defined in a rheological sense) in a reasonable manner. The upper boundary layer does not behave like a rigid plate – the surface velocity varies steadily, instead of being constant. In connection with this fact, the heat flux profile does not agree with the observed ones. DeBremaecker (1977a) discussed possible reasons for this disagreement. He argued that it might be caused by the fact that the surface is not free to move up and down in the model, or that it is assumed to be two dimensional or to be in steady state. However, it seems most likely that it is caused by a too simple rheological behaviour of the model lithosphere, which is assumed to have a high viscosity that is uniform over the whole length of the plate. At the active margins of a plate the behaviour can be quite different from that in the middle of the plate.

Another important point is – although not much attended by the authors – that the upper mantle temperature in the models is considerably lower than the expected one. This may be due to the fact that all these models assume the convection to be restricted to the upper mantle (to about 700 km depth).

The hypothesis that the lithospheric slab (and so the convection current, too) does not enter the lower mantle is mainly supported by the absence of earthquakes below 700 km and by the fact that the stress state in the lower parts of the subducted lithosphere is always compressive. So it is assumed that there is a barrier at about 700 km. Such a barrier could consist of a radial chemical heterogeneity (increased iron content) or of a very steep increase of viscosity at or below the 670 km – discontinuity. However, now there is an increasing opposition to this point of view (Davies, 1977; O'Connell, 1977). A change of iron content in the mantle cannot be excluded, but it is not required by recent mantle models, and the assumption that there is none seems to be favored (Ringwood, 1975, pp. 481–514). Sammis et al. (1977) pointed out that there should not be a large increase of viscosity in connection with the phase boundaries, and Jordan (1977) showed that the lithospheric slab might penetrate the lower mantle at the Kuril trench.

Until now only simple models of whole mantle convection exist, based on boundary layer theory (e.g., Elsasser et al., 1979) or on marginal stability analysis (e.g., Davies, 1977). It seems advisable to carry out fully dynamical models of deep convection and to compare them with shallow convection models. This may lead to further indications which could help decide which of the contradictory hypotheses is right.

So far always finite difference techniques have been used to model mantle convection. This method is well established and easy to implement for special problems. But its accuracy and reliability becomes doubtful when parameters and variables vary greatly from one point of the grid to the next like in the thin boundary layers of the convection cell. Finite element methods are more

accurate, because these quantities are not represented by single points but by continuous test functions.

I developed a finite element method for solving the equations of convection in a fluid with Newtonian position-dependent viscosity. Bicubic (for the stream function) and biquadratic (for the temperature) spline functions are used as test functions on a rectangular grid. Models of mantle convection are presented which have a nearly uniform surface velocity, and heat flux profiles which agree very well with the observed values. Dynamical model calculations are carried out for deep mantle convection and compared with upper mantle models. Special attention is payed to the thermal regime of the mantle and the mantle geotherm.

2. Mantle Temperatures

On the one hand convection models can give valuable indications on the temperature distribution in the mantle. On the other hand there are some observational constraints, which should be fulfilled by the model. Thus we have an important criterion to judge the model, since only little is known about the flow pattern beneath the plates and otherwise only surface features (plate velocity, heat flux, etc.) can be used to compare the model with the real earth. Therefore I shall first review shortly the recent observational knowledge about mantle temperatures.

For the lithosphere, temperatures can be derived from petrological data (pyroxene geothermometry). At the bottom of the oceanic lithosphere at 100 km, the temperature is 950°–1,200° C according to McGregor and Basu (1974) and 1,100–1,250° C according to Mercier and Carter (1975). No oceanic pyroxene data are available for greater depth. For the upper mantle, Tozer (1970) derived the temperature from electrical conductivity data. Assuming an olivine mantle with 10% iron content, he estimated the mean temperature of the uppermost 400 km to be below 1,290° C with a best fit of 1,150° C.

The olivine-spinel phase boundary gives another opportunity to calculate the temperature at its depth, because it is known from laboratory measurements, under which $P-T$-conditions the transition takes place. In this way Fusijawa (1968) derived a temperature of 1,340° ± 190° C for the depth level of about 370 km. Gebrande (1975) got 1,400° ± 100° C and Graham (1970) derived 1,450° ± 150° C, the latter used also information from a petrological model with the according temperature-dependence of the elastic moduli etc.

For the lower mantle only estimates from petrological models are available. These estimates are more insecure because a number of uncertain assumptions have to be made. Concerning the 670/700 km depth level, Graham and Dobrzykowski (1976) calculated the temperature to be 1,600° ± 400° C, and Watt and O'Connell (1978) gave 1550° ± 150° C. The compositional model of Wang (1972) yields temperatures of 2,500° C for 1,300 km, and 3,000° C for 2,800 km depth with an error of ± 800° C.

A last constraint results from the fact that the outer core is liquid, so the temperature at the core-mantle boundary must be above the melting point of the core's iron alloy. The melting temperature depends on the light alloying

element which must be in the core; and because of the very high pressure, only rough estimates from thermodynamic principles can be made. For pure iron Higgins and Kennedy (1971) derived a melting point of 3,750° C at the core-mantle boundary, and Leppaluoto (1972) gave a value which is even 1,000 degrees higher. Silicon as an alloying element would not reduce the melting temperature very much, but sulphur can do so. For the iron-sulphur eutecticum ($\simeq Fe_2S$) Stacey (1977) estimated the melting point to be 2,600° C, and Tolland (1974) gives only 2,260° C. Because the temperature at the core-mantle boundary should be some hundred degrees above the melting point, a minimum temperature constraint of about 2,800° C exists. But - depending on the light element in the core - it might be that temperatures up to 5,000° C are required.

3. Description of the Model

Geometry and Hydrodynamic Conditions

Now the basic design of the model will be explained, and its main idealizations shall be discussed.

A convection cell in a rectangular enclosure - extended infinitely into the third dimension - is to be modelled. The cell shall be connected with an oceanic plate and be part of a periodic scheme of equal convection cells. These simple geometric conditions are required to keep the system practicable, but they imply several unrealistic simplifications:

- It is not likely that the flow pattern beneath the plates is two-dimensional or nearly two-dimensional.
- In the model the descending angle of the plate is 90°, while it is less in reality (15°–90°). Moreover, because of the periodicity, there are two oceanic plates converging against each other and *both* descending into the mantle. Such a behavior cannot be observed anywhere on the earth.
- The surface is not free to move vertically.
- The aspect ratio of the cell is prescribed and not free to adopt a 'natural value'.
- The curvature of the earth is not included. Concerning shallow convection models, this seems not to be so important, but for deep convection it could be of some consequences (see Chaps. 6.4 and 8).

The enclosure is filled with a Newtonian fluid. Its viscosity depends on position - mainly on depth - but it is not controlled by temperature and pressure. This, of course, is a serious simplification, because it is likely that the rheology of the earth's mantle is non-Newtonian and sure that it is strongly temperature-dependent. But the existing models show that the results do not become better if such a rheology is used. They seem to be even worse when the viscosity is not confined to a relative small maximum value for the lithosphere (Houston and DeBremaecker, 1975; DeBremaecker, 1977a). This may be due to a change in deformation mechanism when the temperature becomes too low ($T < 0.5\, T_{melt}$), from steady state creep (diffusion or dislocation creep) to plastic deformation, transient creep, fracture or elastic deformation. Especially in the

lithosphere – in the normal as in the subducted part – these deformation laws could be valid, and the effective viscosities estimated from steady state creep laws are too high. As a simple approximation it is sufficient to use an appropriate chosen depth dependent viscosity. Only for the lithosphere it seems reasonable to introduce also a length dependence, by taking different values for the middle of the plate and for the active margins (see Chap. 6.1).

The boundary conditions usually applied for the flow are 'free slip' at the sides (periodicity!) and at the top, and the no slip condition for the bottom. The latter could be justified by a very steep increase of viscosity at the bottom of the cell, which would also inhibit convection below that boundary. Concerning models of whole mantle convection, 'free slip' is the appropriate condition for the lower boundary, too.

Thermal Conditions

The cell shall be heated by homogeneously distributed (radioactive) inner sources, and by an uniform heat flux from below. That heat may be produced by radioactivity, too, or it may have other sources. Furthermore, frictional heating and the effects of adiabatic compression/decompression will be included as additional sources (or sinks) of heat. The thermal conductivity is mildly temperature dependent, therefore it shall be allowed to vary with depth in the model. The thermal boundary conditions are adiabatic at the sides (periodicity!), $T=0$ at the top, and a specified heat flux at the bottom. The flow is driven by buoyancy forces which are caused by lateral temperature differences via thermal expansion. The effects of phase transitions – both their driving (or hindering) force on the flow and their release of latent heat – will be ignored.

In the model only steady state convection cells are considered. Of course, the convecting mantle of the earth is not in steady state. But the time-dependence of real convection in the earth consists mainly in a change of size and dimensions of the plates (and cells), which cannot be simulated by such simple models at all. To get information about a hypothetical mean convection cell, it seems best to consider the steady state situation.

The model described so far contains a number of grave simplifications (two-dimensionality, steady state, etc.). For that reason its results should not be overestimated, for example by trying to explain peculiarities of special plates with them. But we can hope that they are useful in considering general aspects of plate motion, subplate flow, driving mechanism and especially the thermal regime of the mantle.

4. Equations to Be Solved

The governing equations of convection are (Andrews, 1972):

$$\left(\frac{\partial^2}{\partial x^2}-\frac{\partial^2}{\partial z^2}\right)(\eta(\psi_{xx}-\psi_{zz}))+4\frac{\partial^2}{\partial x\,\partial z}(\eta\,\psi_{xz})=\frac{\partial}{\partial x}(\rho_0 g\,\alpha T)$$

(Hydrodynamic equation)

Table 1. List of symbols

α	Thermal expansivity	Q_{int}	Internal heat generation per unit volume
c_p	Specific heat	ρ_0	Density (mean or reference value)
η	Viscosity	T, T_{abs}	Temperature, absolute temperature
g	Gravity acceleration	$u=\psi_z$	Horizontal velocity
$\kappa=\frac{\lambda}{\rho c_p}$	Thermal diffusivity	$w=-\psi_x$	Vertical velocity
λ	Thermal conductivity	x	Horizontal coordinate
ψ	Stream function	z	Vertical coordinate, pointing upwards
Q_b	Heat flux through the bottom		

$$\frac{\partial T}{\partial t}+u\frac{\partial T}{\partial x}+w\frac{\partial T}{\partial z}-\frac{1}{\rho_0 c_p}\left(\frac{\partial}{\partial x}(\lambda T_x)+\frac{\partial}{\partial z}(\lambda T_z)\right)+w\rho_0\alpha T_{\text{abs}}$$
$$=Q_{\text{int}}+\frac{1}{\rho_0 c_p}(\eta(\psi_{xx}-\psi_{zz})^2+4\eta\psi_{xz}^2).$$

(Energy equation).

These equations are valid for an incompressible fluid with negligible influence for inertia (Prandtl number is infinite). The Boussinesq approximation is made, that means that the density is taken to be constant, except to calculate the buoyancy term in the hydrodynamic equation where it is assumed to depend on temperature only via thermal expansion.

In order to prepare the equations for the numerical procedure, dimensionless variables are introduced, following Torrance et al. (1973). The quantities α, g, and c_p are assumed to be constant, λ is replaced by κ. Only the steady state situation shall be considered, so the term $\partial T/\partial t$ can be omitted. All quantities in the following equations are dimensionless, as defined in Table 2.

$$\left(\frac{\partial^2}{\partial x^2}-\frac{\partial^2}{\partial z^2}\right)(\eta(\psi_{xx}-\psi_{zz}))+4\frac{\partial^2}{\partial x\,\partial z}(\eta\psi_{xz})=Ra\frac{\partial T}{\partial x} \tag{1}$$

$$-\frac{\partial}{\partial x}(\kappa T_x)-\frac{\partial}{\partial z}(\kappa T_z)+uT_x+wT_z+Di\cdot w\cdot T_{\text{abs}}$$
$$=Q_{\text{int}}+\frac{Di}{Ra}\cdot\eta\cdot((\psi_{xx}-\psi_{zz})^2+4\psi_{xz}^2). \tag{2}$$

The boundary conditions are

at the sides	$\psi_{xx}=0$			and	$T_x=0$,
at the top	$\psi_{zz}=0$			and	$T=0$,
at the bottom	$\psi_{zz}=0$	or	$\psi_z=0$	and	$T_z=-Q_b/\kappa$,

and $\psi=0$ on the whole enclosure.

Table 2. Dimensionless quantities. Dimensionless variables are signed by a "¯", the physical variables have none. h, κ_0, T_0, and η_0 are properly chosen reference values

$\bar{x}$	$=x \cdot 1/h$	Coordinates
$\bar{u}$	$=u \cdot h/\kappa_0$	Velocity
$\bar{T}$	$=T \cdot 1/\Delta T_0$	Temperature
$\bar{\kappa}$	$=\kappa \cdot 1/\kappa_0$	Thermal diffusivity
$\bar{\eta}$	$=\eta \cdot 1/\eta_0$	Viscosity
$\bar{\psi}$	$=\psi \cdot 1/\kappa_0$	Stream function
$\bar{Q}_{\text{int}}$	$=Q_{\text{int}} \cdot h^2/(c_p \kappa_0 \Delta T_0 \rho_0)$	Rate of internal heating
$\bar{Q}_b$	$=Q_b \cdot h/(c_p \kappa_0 \Delta T_0 \rho_0)$	Bottom heat flux
Ra	$:=\dfrac{\alpha g \rho_0 \Delta T_0 h^3}{\eta_0 \kappa_0}$	Rayleigh number
Di	$:=\alpha g h/c_p$	Dissipation number

5. Numerical Method

The first attempt to solve the convection problem with a finite element method was made by Sato and Thompson (1976). Their calculation based on the original Navier-Stokes equation instead of the stream function formulation [Eq. (1)], and they used a 'classical' finite element method. The main advantage of the classical method is that it is possible to use an arbitrary irregular grid, this does not seem necessary for the model designed before. Therefore I prefered a spline function approach on a rectangular grid. It has the advantage that the required continuity of the test functions and their derivatives can be easily fulfilled.

The differential operator of the stream function Eq. (1)

$$\hat{L}=\left(\frac{\partial^2}{\partial x^2}-\frac{\partial^2}{\partial z^2}\right)\eta\left(\frac{\partial^2}{\partial x^2}-\frac{\partial^2}{\partial z^2}\right)+4\frac{\partial^2}{\partial x\,\partial z}\left(\eta\frac{\partial^2}{\partial x\,\partial z}\right)$$

is positive definite, so the Rayleigh-Ritz variational principle is applicable. This leads to a system of linear equations (see, for example, Prenter, 1975, pp. 201ff.):

$$A\,x=r \tag{3}$$

with the matrix elements being

$$a_{ij}=\int \psi_i \hat{L}\psi_j\,df \tag{4}$$

and the right hand side vector

$$r_i=Ra\int \psi_i \frac{\partial T}{\partial x}\,df.$$

ψ_i, ψ_j are the test functions and x_i the coefficients of the approximate solution

$$\psi=\sum x_i \psi_i.$$

The integral (4), which contains fourth order derivatives, can be transformed into an expression containing only second order derivatives:

$$\int \psi_i \hat{L} \psi_j \, df = \int \left(\frac{\partial^2}{\partial x^2} \psi_i - \frac{\partial^2}{\partial z^2} \psi_i \right) \eta \left(\frac{\partial^2}{\partial x^2} \psi_j - \frac{\partial^2}{\partial z^2} \psi_j \right) + 4 \frac{\partial^2}{\partial x \, \partial z} \psi_i \left(\eta \frac{\partial^2}{\partial x \, \partial z} \psi_j \right) df.$$

It is sufficient to use test functions which are continuous up to their second derivatives, for that reason bicubic splines with C^2 - smoothness (Prenter, 1975, pp. 131ff.) are used. The matrix A has band structure and is positive definite; therefore only one Cholesky transformation must be done, and then Eq. (3) can easily be solved for any arbitrary temperature field.

The differential operator of the energy Eq. (2) (for fixed values of the velocity field) is not positive definite, thus no variational principle exists. So I take a weighted residual process to solve the equation approximately. This means that the integrals

$$\int \theta_i (\hat{K} T - s) \, df \qquad i = 1, \ldots, n \tag{5}$$

are forced to become zero. $\hat{K}(u, w)$ is the differential operator of Eq. (2), s is the right hand side in (2), T is the approximate solution in spline space, and the θ_i are a set of weighting functions. Usually the weighting functions are chosen equal to the test functions (Galerkin method). The integrals (5), containing second order derivatives, can be transformed by partial integration, they will then contain only first order derivatives. For this reason it is sufficient to take test functions of lower order than for the hydrodynamic equation, and bi-quadratic splines with C^1-smoothness are applied.

In my calculations the Galerkin process proved to be successful only for small Rayleigh numbers, i.e., as long as the convective heat transport is not much more dominant than the conductive transport. But at high Rayleigh numbers ($>3 \cdot 10^4$), (spatial) oscillations occurred in the numerical solution which had the same periodicity as the finite element grid. Concerning the numerical treatment of convective heat transport, a special weighted residual method - similar to the well known 'upwind differencing scheme' in finite difference techniques - seems to be appropriate. As proposed by Zienkiewicz (1977, pp. 633ff.), an upwind finite element method was constructed by composing the weighting function of the normal Galerkin-(test-)function and a special antisymmetric function of higher order (Fig. 1). The antisymmetric function is weighted in a proper manner, dependent on the sign and magnitude of the local velocity field. This procedure made the oscillations disappear.

The numerical grid, which was used for shallow mantle convection models, is shown in Fig. 2. It is composed of 32 elements in length and 11 elements in depth, accordingly it contains 352 elements. In deep mantle models, 5 more elements are added in depth, the total number of elements is then 512. The size of the elements is variable, the vertical extension increases with depth by a factor

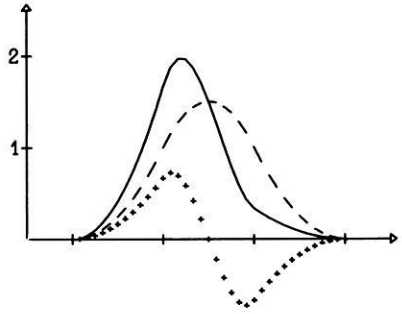

Fig. 1. Example of an one-dimensional weighting function on an equispaced grid for solving the convective heat transfer problem by an 'upwind' finite element method. ------: Normal or Galerkin weighting function (quadratic B-spline); + + + +: antisymmetric weighting function having 2/3 of the possible maximum amplitude; ——: the whole weighting function, being the sum of the other two functions

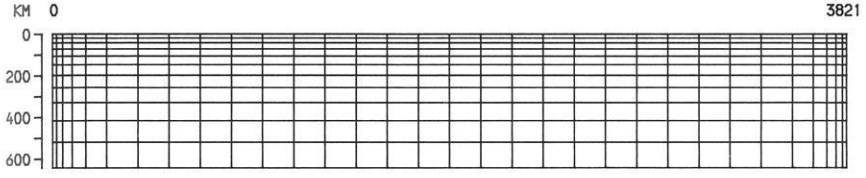

Fig. 2. Numerical grid used in shallow depth models. The mesh is finest in the upper and lateral boundary layers where the variations of stream function and temperature can be expected to be most striking

of 1.2 from one element to the following, starting with 20 km at the top of the lithosphere. The length of the elements remains constant in the middle (150 km), but at the margins it decreases exponentially down to 19.75 km for the last element.

To iterate into steady state, the easiest way is by starting from an initial temperature field, calculating the according velocity field by Eq. (1), and then evaluating by Eq. (2) a new temperature field. Since the $\partial T/\partial t$-term is omitted from Eq. (2), the calculated 'new' temperature field would result if the velocity field would be stationary. But as long as the velocity field has not reached the final state, the procedure has to be repeated: again the velocity field belonging to the last temperature distribution via Eq. (1) is calculated, and with it another improved temperature field, and so on.

But this simple method converged into steady state only when the Rayleigh number was small. At high Rayleigh numbers it was unstable, oscillations occurred which decreased very slowly or were even increasing. Therefore a modified method had to be applied: The calculated 'new' temperatures are replaced for the further calculation by a linear combination of 'old' and 'new' temperatures

$$T = (1-\beta)\, T_{\text{new}} + \beta\, T_{\text{old}}.$$

In deep mantle calculation, the factor β had to be as high as 0.9 to keep the procedure stable. Of course, a large β makes the rate of convergence slow. The need to use such a high 'reduction factor' may indicate that there is no true

stable steady state of convection at very high Rayleigh numbers. Of course, it is only a hope that this forced pseudo steady-state represents the mean situation of true time-dependent convection. However, the hope is encouraged by the observation that in the undamped solutions temperatures and stream function are oscillating just around their values of the damped solution.

The calculation was stopped when both the change in temperatures and in the stream function was at every point less than 0.1 % from one step to the next. Usually a much lower limit is required, this large limit was chosen in order to save computer time. When reducing the limit by one order of magnitude deviations of a few degrees can be observed in the temperature field. Thus steady state is not entirely reached, but it seems to be close enough, especially if one regards that steady state is only an idealization of the model with respect to the real mantle. The deviation between total heat input and surface heat flux, which is less than 1 % in the shallow and less than 3 % in the deep models, might be taken as another measure of the closeness to steady state. However, this may have different reasons, since conservation of energy is not guaranteed perfectly by the numerical procedure.

The reliability and high accuracy of the method was confirmed by comparing different test models with own finite difference calculations and with the results of Torrance et al. (1973) and Houston and DeBremaecker (1975).

6. Parameters of the Model

6.1. Viscosity

Both the linear diffusion creep and the nonlinear dislocation creep have a temperature-pressure dependence following the law

$$\eta = A \cdot T \exp((E^* + p V^*)/RT). \tag{6}$$

E^* = activation energy; V^* = activation volume;
A = proportionality constant.
(in the nonlinear case η must be considered as the effective viscosity and A would be stress-dependent)

In order to construct a viscosity - depth profile, proper values for E^* and V^* are chosen (100 kcal/mol; 10 cm^3/mol above 650 km and 9.5 cm^3/mol below 650 km) and a guess of the temperature - depth profile with regard to the discussion in Chap. 2 was made. The constant A was taken to be 100 Poise/K in order to make the viscosity minimum $3 \cdot 10^{21}$ Poise, which is in good accordance with data from postglacial uplift.

Applied to the lithosphere, Eq. (6) would give values that are too high, rising up to 10^{30} Poise and more above 50 km. For that reason it is only used to calculate the viscosity below 100 km. The profile is continued into the lithosphere in a reasonable manner, reaching a maximum value of $4 \cdot 10^{25}$ Poise at the top and having a mean value of about 10^{24} Poise (Walcott, 1970). The resulting profile is shown in Fig. 3a. Near the spreading center, the lithosphere becomes

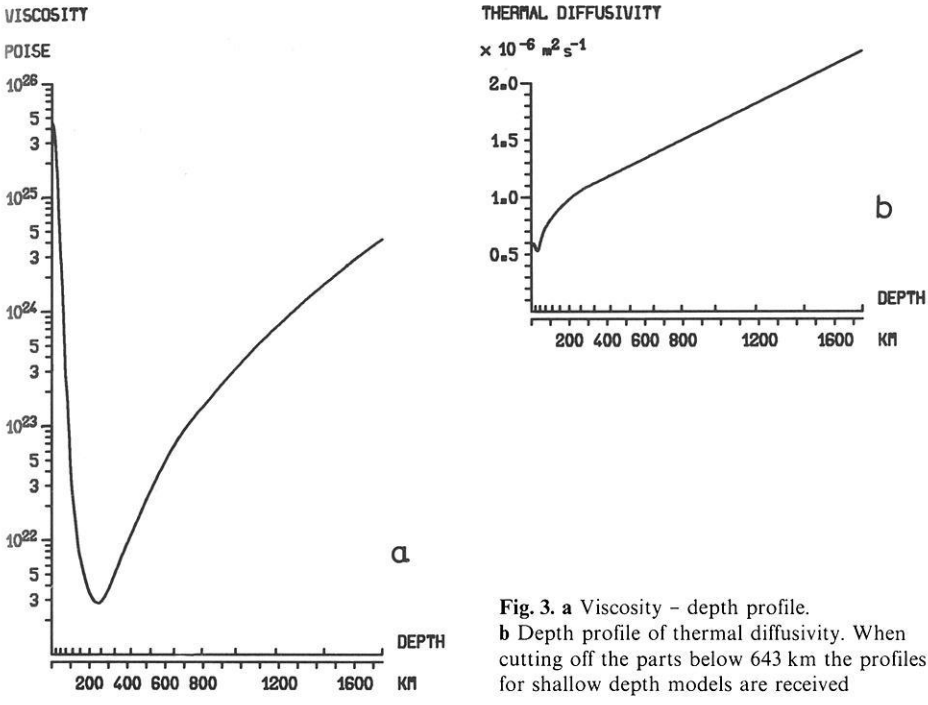

Fig. 3. a Viscosity - depth profile. **b** Depth profile of thermal diffusivity. When cutting off the parts below 643 km the profiles for shallow depth models are received

much thinner, and at the axis itself hot partially molten material rises up nearly to the surface. Therefore a horizontal layering of viscosity seems inappropriate in that region. A 'weak zone' is introduced at the margin, that means that the viscosity in the uppermost 100–150 km is reduced with respect to the normal lithosphere at the middle of the plate. At the spreading center, the asthenospheric minimum value of $3 \cdot 10^{21}$ Poise is continued up to the surface.

In the trench region, another deviation from horizontal layering occurs, because the cold highly viscous lithospheric slab descends at least several hundred kilometers into the mantle. On the other hand, there are some arguments which support the assumption that the effective viscosity is not so high here as in the middle part of the plate. The bending of the plate during the initial stage of subduction can be assumed to produce high stresses. The influence of that increased stress level is difficult to calculate but it is likely that it would lower the effective viscosity. If one assumes an elasto-plastic or brittle lithosphere, the plate would become weaker, since plastic flow, transient creep, or fracture would occur. If - on the other hand - a purely viscous model of the lithosphere with a nonlinear behavior following the law $\dot{\varepsilon} \sim \sigma^3$ is adopted, the effective viscosity is given by

$$\eta_{\text{eff}}(\sigma) = \sigma/\dot{\varepsilon} \sim 1/\sigma^2.$$

Thus it decreases rapidly if the stress level is increased. In the model viscosity distribution the trench region of the lithosphere has a reduced value of about

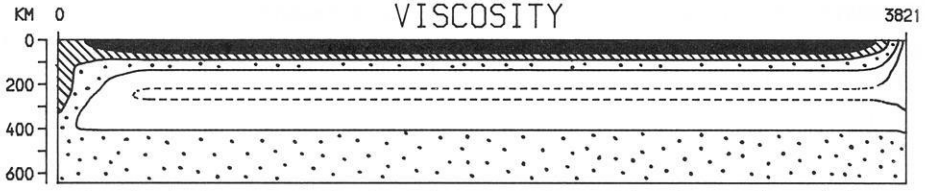

Fig. 4. Viscosity distribution used for the shallow convection models. The spreading axis is on the right and the subduction zone on the left. Viscosity is above 10^{24} Poise in the black area, between 10^{23} and 10^{24} in the hatched, between 10^{22} and 10^{23} in the dotted, and below 10^{22} Poise in the white area. Between the dashed lines in the white region it is below $3 \cdot 10^{21}$ Poise. In deep convection models the same distribution is adopted, completed by horizontally layered viscosity beneath 643 km according to the profile in Fig. 3a

10^{23} Poise. The whole viscosity distribution is shown in Fig. 4. We can hope, that this concept of weak zones leads to a more realistic behavior of the surface plate than in previous models with horizontally layered viscosity (DeBremaecker, 1977a).

6.2. Thermal Diffusivity

The depth dependence of the thermal diffusivity was calculated according to the formulae given by Schatz and Simmons (1972). In order to get better agreement with the experimental results of Kanamori et al. (1968), the term for the photon conductivity was slightly altered (e.g., by taking a higher threshold temperature). In this way we get slightly reduced values in the upper lithosphere and slightly higher values below than by using the original formula. For the oceanic crust, the diffusivity was chosen to have a constant value of $0.6 \cdot 10^{-6}$ m^2/s. The diffusivity profile is shown in Fig. 3b.

6.3. Heat Sources

The total amount of heat generation was determined in order to produce a mean surface heat flux of 1.5 HFU ($62\,mW \cdot m^{-2}$). In the shallow convection model, it is assumed that half of the heat is produced inside the cell and that the other half comes from below, thus assuming that the upper mantle is enriched with radioactive elements. For the deep mantle models, homogeneous distribution throughout the whole mantle is assumed, and the heat flux from the core is fixed to be 10% of the earth's total heat. Then 2/3 of the heat is produced in the cell and 1/3 comes from below. The absolute values are listed in Table 3.

6.4. Depth and Length of the Cell

The depth of the shallow convection cell is limited to 643 km. This is near the spinel-oxide phase boundary ($\simeq 670$ km) which might possibly confine the depth of upper mantle convection.

The depth in deep mantle convection models is 1,748 km which is about 60% of the mantle depth. This arbitrary confinement ('intermediate convection model' in a medium position between upper mantle and whole mantle convection) is mainly done in order to restrict the computational expense. It would be justified if the high viscosity in the lower mantle would cause that the return flow penetrates only intermediate depth or plays only a minor role in the lowermost mantle.

However, in some manner this model may nevertheless be considered as a model of whole mantle convection. That is because a 1,750-km-deep plane mantle has nearly the same volume as a 2,900-km-deep spherical mantle with the same surface area. In mantle convection the heating of the cell is mainly a volume process, but the cooling is a surface process. If a flat mantle model is used instead of a spherical mantle, it seems best from the thermal point of view to choose the surface and the volume equal to the spherical values.

Of course, in the spherical geometry the stream pattern would be changed which influences the temperatures as well. Therefore the interpretation of the model as whole mantle convection remains doubtful – some consequences are mentioned in the discussion part (Chap. 8). However, I assume that – if you want to avoid the several difficulties connected with a spherical model and use a plane model – it is better to adjust the volume to the true value and not the depth extent.

The length of the cell is fixed to be 3,821 km. This is about the intermediate range of the earth's plates, for example the Nazca plate is approximately of this length.

6.5. Velocity of the Plate

The mean plate (or surface) velocity is, of course, not an input parameter of the model. But to make the different models comparable, they should have a similar plate velocity. Furthermore, to make reasonable statements about the mantle temperatures, the plate velocity should have a value which may be considered as the mean value of the earth's plate system.

This mean value is determined as follows: The annual rate of sea-floor spreading over the whole earth is about 2.0–3.5 km^2/a, Dickinson and Luth (1971) assume 1.7–2.3 km^2/a, Bickle (1978) gives 2.7–3.3 km^2/a and Garfunkel (1975) calculated 3.15 km^2/a. If a value of 2.9 km^2/a is taken and the earth's surface area is divided by it, we get as mean overturn time of a lithospheric plate 176 m.y. The 3,821-km-long model plate shall have the same overturn time and thus a velocity of 2.17 cm/a.

The Rayleigh number in my model calculations was always fitted in such a way that a mean surface velocity between 2.1 and 2.2 cm/a resulted. This is allowed since the mean viscosity of the earth's (upper) mantle is uncertain in several orders of magnitude. In all the models the Rayleigh number had to be increased by a factor of about 4 compared with its standard value, corresponding to a reduction of the all-over-viscosity by a factor of 4 with respect to the profile shown in Fig. 3a.

Table 3. List of model parameters. If more than one value is given the first belongs to the shallow model and the second to the deep model. The appendix "*ref.*" means "reference value"

Depth	h	$= \frac{643}{1748}$ km	$= \frac{0.643}{1.748} \cdot 10^6$ m
Length	1	= 3821 km	$= 3.821 \cdot 10^6$ m
Aspect ratio	1/h	$= \frac{5.95}{2.19}$	
Viscosity, ref.	η_0	$= 10^{22}$ Poise	$= 10^{21}$ kg m^{-1} s^{-1}
Thermal diffusivity, ref.	κ_0	=	10^{-6} m^2 s^{-1}
Density, ref.	ρ_0	= 3.8 g/cm^3	$= 3.8 \cdot 10^3$ kg m^{-3}
Specific heat	c_p	= 0.287 cal/(g · grd)	$= 1.2 \cdot 10^3$ J kg^{-1} K^{-1}
Thermal expansivity	α	=	$3.0 \cdot 10^{-5}$ K^{-1}
Temperature difference, ref.	ΔT_0	=	2000 K
International heat production	Q_{int}	=	$\frac{4.88}{2.39} \cdot 10^{-8}$ W m^{-3}
Bottom heat flux	Q_b	$= \frac{0.75}{0.50}$ HFU	$= \frac{31.4}{20.9} \cdot 10^{-3}$ W m^{-2}
Rayleigh number, standard value	Ra_s	$= \frac{606155}{12195155}$	
Dissipation number	Di	$= \frac{0.1608}{0.4372}$	

6.6. Other Parameters

The other parameters of interest are less critical. In Table 3 all the parameters are listed.

7. Results

7.1. Shallow Mantle Convection (Model No. 20)

The results of the shallow mantle convection model is shown in Figs. 5–7, special values of interest are listed in Table 4 for all the models.

Surface Velocity and Heat Flux (Fig. 5). Except for the 260-km-wide marginal regions, the surface velocity is nearly uniform. It increases slightly towards the trench region, but only by 3%. The surface boundary layer in the model can be considered as a rigid plate in a very good approximation. Whether there is a slight deformation of real plates by travelling insignificantly faster near the trench cannot be resolved, but it does not seem impossible.

The heat flux profile is in good agreement with the 'reliable' heat flux averages for the North Pacific from Sclater and Crowe (1976) (rectangles in Fig. 5b).

Stream Pattern (Fig. 6a). The ascending and descending flow is restricted to narrow boundary layers; the ascending flow is even narrower and faster than the downgoing (maximum velocity 9.3 cm/a in the upwelling limb). Outside the

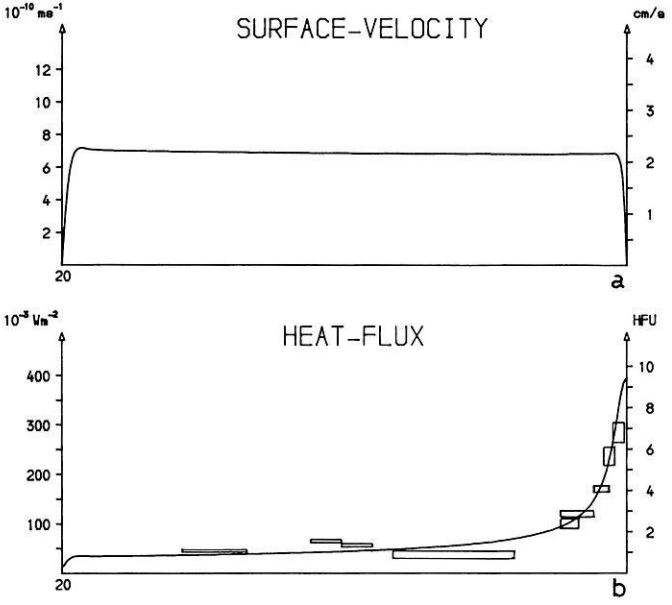

Fig. 5a and b. Model 20: Surface velocity **a** and surface heat flux **b** measured over the length of the plate. The spreading center is on the right. The rectangles in **b** are the 'reliable' heat flux averages from Sclater and Crowe (1976). Their original dependence on age was converted into length dependence using a constant plate velocity of 2.15 cm/year

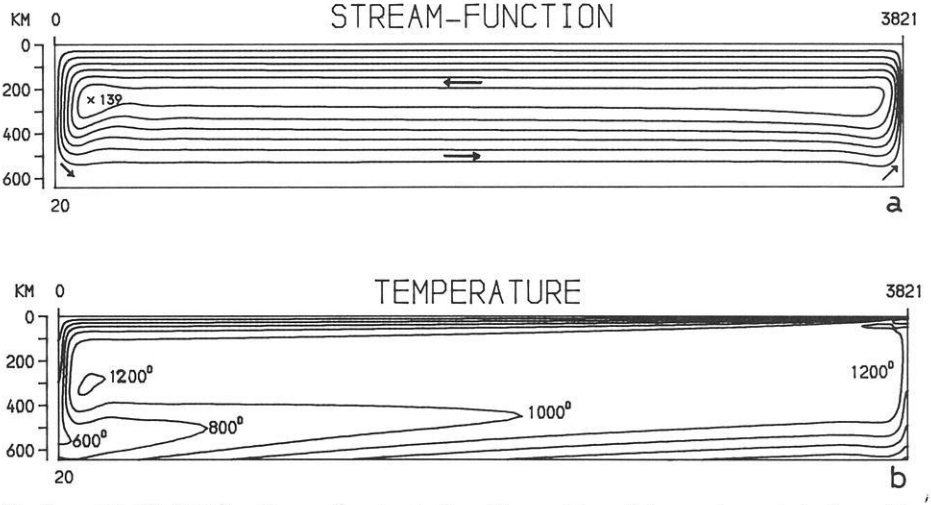

Fig. 6a and b. Model 20: **a** *Stream function isolines.* The position of the maximum is designated by an *x*. Lines are drawn every 20 (dimensionless) units. **b** *Temperature isolines.* Temperature is in °C, every 200° one line is drawn

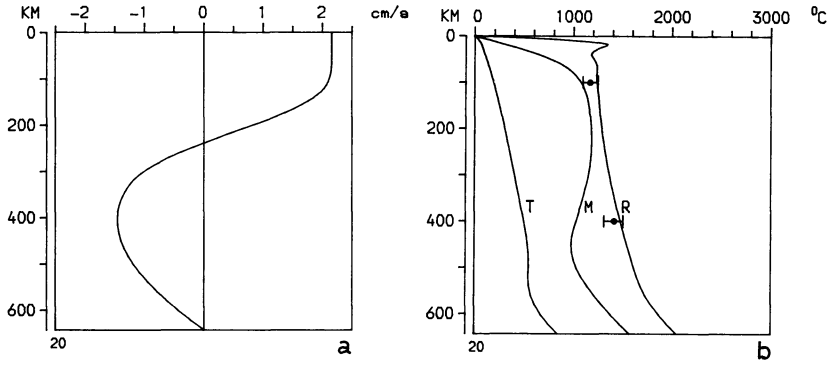

Fig. 7a and b. Model 20: **a** *Depth profile of horizontal velocity.* The profile is taken in the middle of the cell at half the length between spreading center and subduction zone. **b** *Temperature-depth profiles.* The profiles are taken in the trench region (*T*) at the length $l = 0$ km, in the middle of the cell (*M*) at $l = 1910$ km, and at the ridge (*R*) at $l = 3821$ km. Over most of the horizontal extent of the cell the profile is similar to the middle geotherm, only at the margins significant deviations occur. The following 'observational' values are included: 100 km: 1,100°–1,250° (Mercier and Carter, 1975) pyroxene-geothermometry; 400 km: 1,300°–1,500° (Gebrande, 1975) olivine-spinel-transform.

marginal regions, the flow is nearly horizontal, the vertical velocity remains below 0.1 cm/a almost everywhere.

In Fig. 7a the depth profile of the horizontal velocity in the middle of the cell is shown. The velocity remains constant in the lithosphere down to 100 km and then it begins to decrease. This contradicts the idea that the plate might be driven by an asthenospheric flow because in this case the velocity should first *increase* below the plate. The depth of reversal, where the plate - directed flow turns into a counter flow, is 240 km which is very near the depth of the minimum of viscosity (245 km).

Temperatures (Figs. 6b and 7b). The temperature field is characterized by a steep increase with depth in the lithosphere, an almost isothermal region from the bottom of the plate down to about 350 km over nearly the whole length of the cell, narrow boundary layers at the margins and a warm boundary layer at the bottom. A tongue of cold material extends horizontally from the descended lithosphere into the cell at a depth of 400–550 km.

The temperature at the bottom of the lithosphere (1,100° C at 100 km depth in the middle of the cell) is in good accordance with the values derived from pyroxene geothermometry (see Chap. 2). This may especially indicate that the values of thermal conductivity in the lithosphere are well chosen. But the temperatures at greater depths are too low: The mean temperature at 400 km is 1,040° compared with the most realistic value of 1,350°–1,450° C. An important feature of the temperature distribution is an inversion (negative temperature gradient with the z-axis pointing down) which appears between approximately 200 and 550 km depth over most of the cell's length.

Both the inversion of the temperature gradient and the low temperatures at the 400-km level are produced because the cold descending lithosphere does not

heat up enough before beginning the return flow. Such a temperature inversion has important consequences, because it would inhibit small scale convection in the asthenosphere as it is proposed by Richter (1973) and Richter and Parsons (1975). They assumed long Rayleigh-Bénard rolls which are oriented perpendicular to the main flow connected with the plate motion. But these convection cells require of course a superadiabatic gradient which does not occur in this model.

7.2. Alternative Shallow Convection Models (Nos. 21 and 22)

So far the shallow convection model is quite satisfactory in reproducing the main features of plate tectonics and upper mantle dynamics as they are known today, but its mantle temperatures are too low. The difference to realistic values is too great (300°–400°) to be tolerated. Therefore in the following two models attempts were made to raise the temperature by certain modifications.

The thermal conductivity in the mantle is slightly uncertain, especially the influence of photon conductivity. In model 21[1] a reduction of the conductivity by a factor of 0.8 was made ($\kappa_0 = 0.8 \cdot 10^{-6}\,m^2/s$). This size of reduction seems to be within a reasonable range. In the case of purely conductive heat transfer it would rise the temperature by 25% all over. But in the model, the increase was less, the temperature rose about 160° beneath the plate, to 1,260° at the bottom of the lithosphere and to 1,200° C at 400 km. The latter value is still too low and the first value seems even to exceed slightly the range of pyroxene temperatures. Neither the stream pattern nor the general features of the temperature field are changed significantly compared with model 20.

In model No. 22[1] the heat sources were redistributed, assuming a constant rate of heat production in the whole mantle. Then 32% of the total amount of heat is produced inside the cell and 68% is coming from below. The mean temperature at 400 km *sank* to 1,015° C while the temperature at 100 km depth rose by 10° to 1,110°. The result seems to be paradox, but it can be explained by considering the increased velocity of the ascending limb (see Table 4). The additional heat from the bottom is transported more efficiently to the surface or into the lithosphere. The lack of internal heating on the other hand slightly reduces the temperature at intermediate depth. It can be stated that neither a redistribution of heat sources according to uniform heat production nor a change of thermal conductivity improves the upper mantle convection model.

7.3. Deep Mantle Convection Models (Nos. 30 and 31)

In model 30 the depth of the cell is increased to 1,748 km, but for the bottom the no slip boundary condition is applied, considering that perhaps the increase of viscosity in the lower mantle would inhibit flow in the lowermost mantle.

---

[1] Without figure, for further results see Table 4

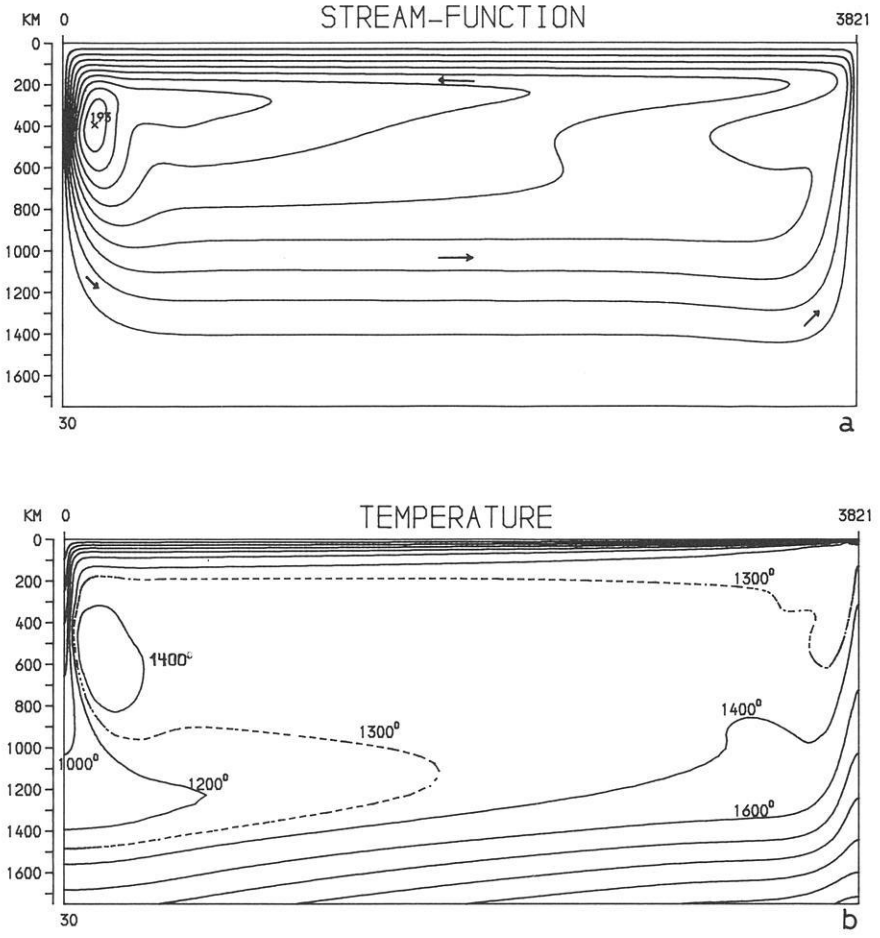

Fig. 8a and b. Model 30: **a** Stream pattern and **b** temperature field. One line is drawn every 20 units in **a** and every 200° in **b** respectively

The stream pattern (Fig. 8a) is now more complicated than in the shallow convection models. The maximum of the stream function is near the descending slab and much more striking, because an additional curl of flow is induced here. In the descending limb the flow is very rapid. The return flow is concentrated mainly between 800 and 1,500 km depth (Fig. 9a), while the reversal of flow (plate flow ↔ return flow) takes place between 200 and 300 km, which is nearly the same depth as in the shallow models. Between 400 and 800 km the return flow is quite slow and the flow tends to move upwards in this depth range even outside of the ridge region.

The surface velocity increases in this model by 11.5% over the length of the plate towards the trench. This value still seems to be tolerable for considering the surface layer as a rigid plate. This variation of velocity implies strong tensile stresses in the plate (see Fig. 10). Thus the plate should be mainly driven by the

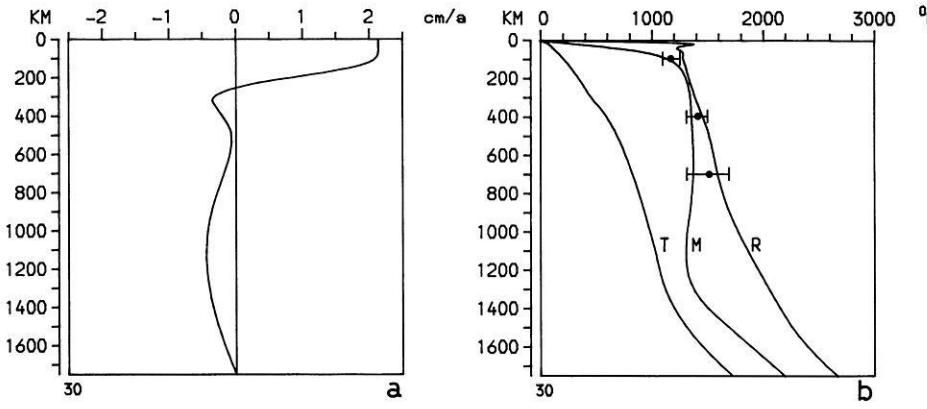

Fig. 9a and b. Model 30: **a** *Velocity-depth profile.* **b** *Temperature-depth profile,* T = trench region, M = middle, R = ridge region. Reference temperatures are included: 100 km: 1,100°–1,250° (Mercier and Carter, 1975) pyroxene-geothermometry; 400 km: 1,300°–1,500° (Gebrande, 1975) olivine-spinel-transformation; 700 km: 1,400°–1,700° (Watt and O'Connell, 1978) petrological model

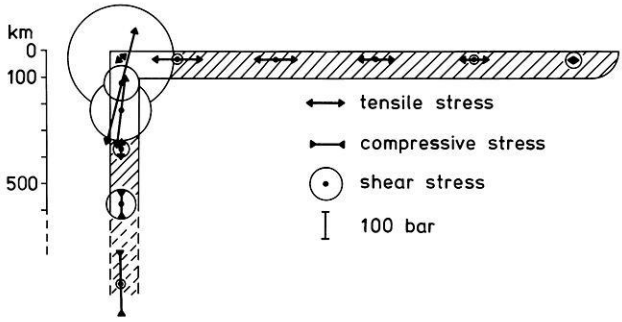

Fig. 10. Model 30: *Stress distribution in the lithosphere.* The plate is drawn schematically, the horizontal scale is reduced by a factor of 2. The normal stress in direction of the flow and the related shear stress are shown at 32 km depth (or distance from the edge of the subducted plate). It can be noted that the stress level is highest in the bending region of lithospheric subduction. This supports the argumentation for the reduction of viscosity in this region (see Chap. 6)

pull of its subducted part. Moreover, the stream pattern suggests that this pull is the main driving source of the flow in the whole cell. The heat flux profile differs only negligibly from the profiles of shallow mantle convection.

The temperature-depth profile is now much more satisfactory in the upper mantle (Fig. 9b). The mean temperature at 100 km depth is 1,180° and at 400 km 1,350° C, the mean value of the whole uppermost 400 km is 1,170° compared with the best value of 1,150° from electrical conductivity data (Tozer, 1970). These values are in good agreement with the data derived from observations, as discussed in Chap. 2. But in the lower mantle temperatures are below the classical estimates. Between 250 km and 1,225 km the temperature gradient is subadiabatic and in some parts even negative, and at 1,100 km depth there is a

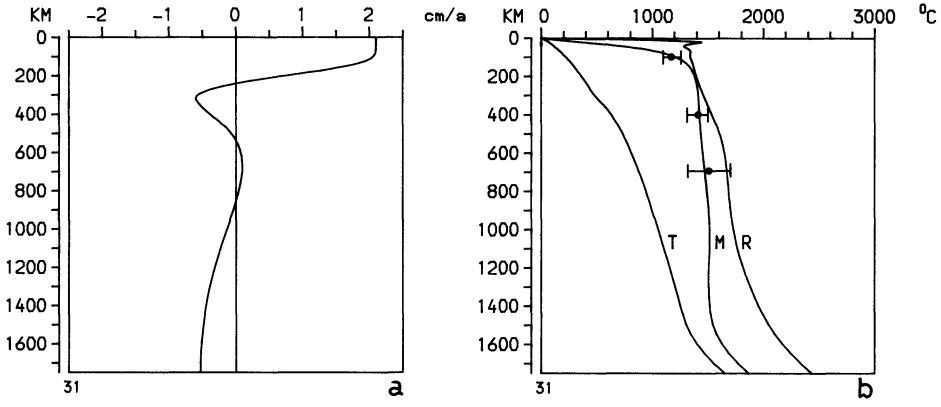

Fig. 11a and b. Model 31: **a** *Velocity-depth profile.* **b** *Temperature-depth profile,* T = trench region, M = middle, R = ridge. The same reference temperatures as in Fig. 9b are included. Compared with model 30 the boundary condition at the bottom is converted from 'no slip' to 'free slip'

minimum in the $T(z)$-profile of 1,300° C. At the bottom the mean temperature is 2,170° C.

It appears strange that there is a slight minimum of temperature in the upper mantle just beside the ascending flow beneath the ridge (Fig. 8b). It can be explained as follows: The cold tongue, extending from the subducted lithosphere on the left into the cell, does not heat up enough because of the very slow conductive heat transfer. When ascending again, it cools because of the adiabatic decompression, and it is then colder than the surrounding mantle. This cool lump near the spreading region seems to produce the strange stream pattern in the right side of the cell.

It was pointed out in Chap. 6.4 that a 1,750-km-deep convection model of a plane mantle may be considered to be similar to a 2,900-km-deep spherical mantle. For whole mantle convection, the boundary condition at the bottom shall be free slip. Thus in the next model everything remains unchanged, except a free slip condition at the bottom instead of 'no slip'. The stream pattern of model 31 is similar to the previous model, except for a greater depth-extent of the return flow which is concentrated between 1,000 km and the bottom. The general pattern of the temperature field is similar, too, except for a less developed lower boundary layer.

The maximum velocity of the return flow appears at the bottom (Fig. 11a). For that reason it is demonstrated that a viscosity of more than 10^{24} Poise in the lower mantle is not sufficient to confine convection to the upper mantle or even to concentrate the return flow at intermediate depth. Therefore the idea of 'intermediate depth mantle convection' (Chap. 6.4) seems to be very doubtful. From this point of view model 31 – considered to be similar to a whole mantle convection cell – seems to be more realistic than model 30 as an intermediate depth cell.

In model 31 the temperatures are slightly higher in most parts of the cell than in model 30 (Fig. 11b). At 400 km a mean temperature of 1,420° C is

Table 4. Model results

Model number	20	21	22	30	31
	Upper mantle convection			Deep mantle convection	
Pecularity	–	λ Reduced	Redistribut. heat sources	–	Free slip at the bottom
Ra/Ra_s	3.88	4.75	3.46	3.94	3.69
ψ_{max}	139	186 (149)	163	193	197
$\bar{v}_p$	2.17	2.18	2.15	2.15	2.11
v_d	−4.8	−5.7	−4.5	−8.3	−8.3
v_a	9.3	9.6	11.4	5.8	4.7
v_r	−1.46	−1.41	−1.44	−0.44	−0.53
Δv_p	3.1%	7.1%	0.7%	11.5%	12.1%
z_{rev}	239	238	238	254	242
T_{100}	1,100°	1,261°	1,109°	1,179°	1,247°
T_{400}	1,040°	1,200°	1,015°	1,350°	1,420°
T_{bot}	1,525°	1,695°	1,730°	2,170°	1,876°

Ra/Ra_s: Ratio between the actual Rayleigh number and its standard value
ψ_{max}: Maximum value of stream function $\bar{v}_p$ mean plate velocity in cm/year
v_a, v_d, v_r: Maximum velocity of ascending, descending and return flow in cm/year
Δv_p: Variation of the plate velocity over the plate length, the 260 km wide marginal regions are excluded
z_{rev}: Depth of reversal of flow direction in the middle of the cell (in km)
T_{100}, T_{400}, T_{bot}: Mean temperature at 100, 400 km depth and at the bottom (in °C)

reached, and in the lower mantle the gradient is slightly higher and the temperatures are about 200° above those of the previous model. But still the gradient is subadiabatic below 240 km down to about 1,450 km. The temperature at the bottom of the cell has a mean value of 1,880° which is by all means below the solidus of the core's material.

8. Conclusions and Discussion

Stream Pattern

The concept of weak zones at the active plate margins proved to be successful to make the highly viscous surface layer behave like a rigid plate. There are some plausible arguments to reduce the effective viscosity not only at the spreading center but also in the subduction region, but the weak zones have still to be justified by a more sophisticated model which regards the complicated temperature and stress controlled rheology of the lithosphere, which is not yet known in detail.

A viscosity of more than 10^{24} Poise in the lower mantle is not sufficient to inhibit deep mantle convection (this is already known from marginal stability analysis, too), but moreover, a moderate increase of viscosity with depth (by 3 orders of magnitude from the minimum to the bottom) cannot concentrate the

return flow to intermediate depth. Thus it seems very likely that the lower mantle is in convection if there are no other inhibiting factors, for example chemical heterogeneity.

The lack of earthquakes below 700 km may be caused by the transformation to a mixed-oxide or perovskite structure at about this depth. A changed mechanical behaviour or the elevated temperatures due to the transformation might remove the slab material out of its brittle region (Davies, 1977; O'Connell, 1977). The predominant compressive stress in the lower parts of the subducted plate must not indicate a barrier at 700 km. In fact the stress state in the descending flow is compressive below 450 km in the deep mantle models and below 350 km in the upper mantle model (see Fig. 10). However, reliable statements concerning this topic would require a model which simulates the descending behavior of the plate better than the present one.

Temperatures

The temperatures at the bottom of the lithosphere agree well with the data derived from pyroxene geothermometry for both the upper mantle and the deep convection model. In the upper mantle below the lithosphere differences occur: The deep convection models satisfy quite well the observational constraints (electrical conductivity, olivine-spinel transformation, petrological data), while in the shallow convection models the temperatures are too low, at the 400 km depth level by 300°–400°. From this point of view it seems very likely that convection is not confined to the upper mantle but is present throughout the whole mantle.

In all the models there is a subadiabatic temperature gradient at intermediate depth. In probably the best model (No. 31) the gradient is higher than in all the others, but it is still below the adiabatic gradient for depths greater than 250 km. If this is true in the mantle, there is only little foundation for small scale convection cells proposed by Richter (1973) and others. A type of small-scale convection initiated by boundary layer instability (Parsons and McKenzie, 1978) might still be possible, but it is doubtful whether it plays an important role, since it would hardly have a big depth-extent and since the Rayleigh number does not exceed its critical value very much.

Some difficulties still remain because of the cool lower mantle in the models. The liquidus of the outer core alloy must be exceeded. This is a strong constraint to the temperatures in the lowermost mantle. Even with the optimal composition (Fe_2S) the temperature at the core-mantle boundary should be at least 2,500° C, but it is more likely that the limit is even higher. Therefore the temperatures at the bottom of the deep mantle models are several hundreds or a thousand degrees below the required values. Several circumstances, which are not regarded in the models, may contribute to raise the temperature of the lower and lowermost mantle.

(a) The olivine-spinel phase boundary has a positive Clapeyron slope. This implies the release of latent heat when material crosses the boundary down-

wards and the lower mantle would be heated. A temperature rise in the order of 100° can be estimated.

(b) Higher temperatures in the lower mantle can be expected if the correct spherical geometry and the true depth of 2,900 km are included in the model. The rise of temperature with increasing depth of the convection cell is shown by comparison between shallow and deep convection models. But another special effect concerning the lower boundary layer results. A spherical mantle sector has only 30% of its surface area at the bottom while the top and bottom area are equal in the plane model. Therefore the same amount of heat coming from the core would imply a heat flux (per unit area) thrice the high in a spherical model, and the thermal gradient at the bottom would be thrice the gradient of the flat earth model. Thus a significant heat flux from the core is producing an important temperature rise in the lower thermal boundary layer of the cell, which might protect the outer core from the low temperatures in the mantle.

The D″-layer at the bottom of the mantle may be identified as this lower boundary layer (Jones, 1977). The other possible interpretation of the D′-layer as chemically different from the rest of the mantle (e.g., iron-enriched) also leads to a shielding of the core from low mantle temperatures because in this case it could not participate in convection. The core's heat must then be transported throughout it by conduction and also a steep temperature rise would be the consequence.

(c) The low model temperatures at the bottom can be caused by the symmetric lateral boundary conditions, which lead to double dipping slabs. Thus the two plates shield each other from the warm surrounding mantle and those parts which finally reach the bottom remain coldest. (One might argue that the whole temperature distribution, including subadiabatic gradients and low temperatures in the lower mantle, would be changed in favor of higher values, if there would be a single descending slab. Of course, the slab is then heated from both sides. However, it must be considered that the rate of subduction always equals the spreading rate and therefore the single slab has to have twice the descending velocity of the double slabs, and the increased heating would be compensated).

It does not seem likely that all these effects would raise the temperature by considerably more than a thousand degrees. Thus temperatures in the lower mantle would remain quite low, and at the core-mantle boundary about 3,000° C can be expected. Therefore the model results support the hypothesis of sulphur being the light alloying element in the core.

Another difficulty arising from such low temperatures in the mantle is the high viscosity which would result from Eq. 6. The increase of viscosity due to the rising pressure can not be compensated by rising temperature. But theoretical considerations suggest that the activation volume does not remain constant but decreases considerably with increasing pressure. According to Sammis et al. (1977), it falls from 11 cm^3/mol at the surface down to 2.5–5 cm^3/mol at the bottom of the mantle. Thus the effect of pressure could be less important and the viscosity could remain low enough to allow whole mantle convection despite the rather low temperature in the lower mantle.

Acknowledgement. I am grateful to the Deutsche Forschungsgemeinschaft, which is financing my work.

References

Andrews, D.J.: Numerical simulation of sea-floor spreading. J. Geophys. Res. **77**, 6470–6481, 1972

Bickle, M.J.: Heat loss from the earth: a constraint on Archean tectonics from the relation between geothermal gradients and the rate of plate production. Earth Planet. Sci. Lett. **40**, 301–315, 1978

Davies, G.F.: Whole-mantle convection and plate tectonics. Geophys. J. R. Astron. Soc. **49**, 459–486, 1977

DeBremaecker, J.-Cl.: Convection in the earth's mantle. Tectonophysics **41**, 195–208, 1977a

DeBremaecker, J.-Cl.: Is the oceanic lithosphere elastic or viscous? J. Geophys. Res. **82**, 2001–2004, 1977b

Dickinson, W.R., Luth, W.C.: A model for plate tectonic evolution of mantle layers. Science **174**, 400–404, 1971

Elsasser, W.M., Olson, P., Marsh, B.D.: The Depth of Mantle Convection. J. Geophys. Res. **84**, 147–155, 1979

Fusijawa, H.: Temperature and discontinuities in the transition layer within the earth's mantle: geophysical application of the olivine-spinel transition in the Mg_2SiO_4—Fe_2SiO_4 system. J. Geophys. Res. **73**, 3281–3294, 1968

Garfunkel, Z.: Growth, shrinking, and long-term evolution of plates and their implications for the flow pattern in the mantle. J. Geophys. Res. **80**, 4425–4432, 1975

Gebrande, H.: Ein Beitrag zur Theorie thermischer Konvektion im Erdmantel mit besonderer Berücksichtigung der Möglichkeit eines Nachweises mit Methoden der Seismologie. Universität München: Diss. Inst. für Allgemeine und Angewandte Geophysik, 1975

Graham, E.K.: Elasticity and composition of the upper mantle. Geophys. J. R. Astron. Soc. **20**, 285–302, 1970

Graham, E.K., Dobrzykowski, D.: Temperatures in the mantle as inferred from simple compositional models. Am. Mineral. **61**, 549–559, 1976

Higgins, G., Kennedy, G.C.: The adiabatic gradient and the melting point gradient in the core of the earth. J. Geophys. Res. **76**, 1870–1878, 1971

Houston, M.H., DeBremaecker, J.-Cl.: Numerical models of convection in the upper mantle. J. Geophys. Res. **80**, 742–751, 1975

Jones, G.M.: Thermal interaction of the core and the mantle and long-term behaviour of the geomagnetic field. J. Geophys. Res. **82**, 1703–1709, 1977

Jordan, T.H.: Lithospheric slab penetration into the lower mantle beneath the Sea of Okhotsk. J. Geophys. **43**, 473–496, 1977

Kanamori, H., Fujii, N., Mizutani, H.: Thermal diffusivity measurements of rock-forming minerals from 300° to 1100° K. J. Geophys. Res. **73**, 595–605, 1968

Leppaluoto, D.A.: Melting of iron by significant structure theory. Phys. Earth Planet. Inter. **6**, 175–181, 1972

McGregor, I.D., Basu, A.R.: Thermal structure of the lithosphere: a petrological model. Science **185**, 1007–1011, 1974

McKenzie, D.P., Roberts, J.M.: Convection in the earth's mantle: towards a numerical simulation. J. Fluid Mech. **62**, 465–538, 1974

Mercier, J.-Cl., Carter, N.L.: Pyroxene geotherms. J. Geophys. Res. **80**, 3349–3362, 1975

O'Connell, R.J.: On the scale of mantle convection. Tectonophysics **38**, 119–136, 1977

Parsons, B., McKenzie, D.: Mantle convection and the thermal structure of plates. J. Geophys. Res. **83**, 4419–4430, 1978

Prenter, P.M.: Splines and variational methods. New York: John Wiley and Sons 1975

Richter, F.M.: Convection and large scale circulation of the mantle. J. Geophys. Res. **78**, 8735–8745, 1973

Richter, F.M., McKenzie, D.: Simple plate models of mantle convection. J. Geophys. **44**, 441–471, 1978

Richter, F.M., Parsons, B.: On the interaction of two scales of convection in the mantle. J. Geophys. Res. **80**, 2529–2541, 1975

Ringwood, A.E.: Composition and petrology of the earth's mantle. New York: McGraw-Hill 1975
Sammis, C.G., Smith, J.C., Schubert, G., Yuen, D.A.: Viscosity-depth profile of the earth's mantle: effects of polymorphic phase transitions. J. Geophys. Res. **82**, 3747–3761, 1977
Sato, A., Thompson, E.G.: Finite element models for creeping convection. J. Comput. Phys. **22**, 229–244, 1976
Schatz, J.F., Simmons, G.: Thermal conductivity of earth materials at high temperatures. J. Geophys. Res. **77**, 6966–6983, 1972
Schubert, G., Froidevaux, C., Yuen, D.A.: Oceanic lithosphere and asthenosphere: thermal and mechanical structure. J. Geophys. Res. **81**, 3525–3540, 1976
Sclater, J.G., Crowe, J.: On the reliability of oceanic heat flow averages. J. Geophys. Res. **81**, 2997–3006, 1976
Stacey, F.D.: A thermal model of the earth. Phys. Earth Planet. Inter. **15**, 341–348, 1977
Tolland, H.G.: Thermal regime of the earth's core and lower mantle. Phys. Earth Planet. Inter. **8**, 282–286, 1974
Torrance, K.E., Turcotte, D.L., Hsui, A.T.: Convection in the earth's mantle. In: Methods in computational physics, Vol. 13, B.A. Bolt, ed.: pp. 431–454. New York, London: Academic Press 1973
Tozer, D.C.: Temperature, conductivity, composition and heat flow. J. Geomagn. Geoelectr. **22**, 35–51, 1970
Walcott, R.I.: Flexural rigidity, thickness, and viscosity of the lithosphere. J. Geophys. Res. **75**, 3941–3954, 1970
Wang, C.Y.: Temperature in the lower mantle. Geophys. J. R. Astron. Soc. **27**, 29–36, 1972
Watt, J.P., O'Connell, R.J.: Mixed-oxide and perovskite-structure model mantles from 700–1200 km. Geophys. J. R. Astron. Soc. **54**, 601–630, 1978
Zienkiewicz, O.C.: The finite element method, 3rd edn. London: McGraw-Hill 1977

Received February 19, 1979; Revised Version June 22, 1979; Accepted August 10, 1979